JOURNAL OF CATALYSIS 123, 86–97 (1990)

Bimetallic Reforming Catalysts: EXAFS Investigation of the Particle-Growing Process during the Reduction Step

D. BAZIN,* H. DEXPERT,* J. P. BOURNONVILLE,† AND J. LYNCH†

*Laboratoire pour L'Utilisation du Rayonnement Electromagnétique (LURE), Bâtiment 209D, Centre Universitaire Paris-Sud, 91405 Orsay, France; and †Institut Français du Pétrole, BP 311, 92506 Rueil-Malmaison, France

Received July 29, 1988; revised July 17, 1989

EXAFS has been used to study the reduction which leads to the active species of Pt–Rh and Pt–Re reforming catalysts. The first moments of the formation of the metallic cluster have been followed kinematically at the platinum absorption edge for two catalysts, Pt–Rh/γ-Al_2O_3 and Pt–Re/γ-Al_2O_3, using two different modes for the EXAFS setup (different synchrotron stations). The experiments have been made *in situ*, the sample being under flowing hydrogen at high temperature. The main result is the appearance of long metal–metal distances, of the same range order as that of the bond lengths existing in the alumina network. They occur solely for a very low number of metal atoms and are probably due to an intergrowth process with the carrier. The phenomenon seems to be general and disappears with the growth of the particle.

INTRODUCTION

In the field of oil reforming, an important number of industrial processes involve heterogeneous catalysts made up of small aggregates supported by light oxides (alumina, silica) of high specific area (200 m^2 g^{-1} or more). In order to increase the efficiency of these catalysts, the metal clusters are extremely small (average size less than 10 Å) and the metal concentrations rarely exceed 1 or 2% in weight.

The numerous results already published in this field (see, for example, Refs. *1–4*) demonstrate that EXAFS is a very efficient tool for studying such materials. In previous papers (*5, 6*), we have discussed the case of Pt–(Re or Rh)/Al_2O_3, and models explaining the fixation of the metal precursors during the first steps of the preparation procedure, drying and calcination, have been suggested. Investigations have also been made of the reduction step, either after the reaction took place (*7*) or during the activation procedure (*8*). We recently focused on the intermediate states which occur at the very beginning of the reduction process (*9*). The main result we found in the case of the monometallic Pt/γ-Al_2O_3 catalyst (i.e., H_2PtCl_6 on γ-alumina) was that the growth of the platinum cluster is related to the geometry of the carrier through oxygen bonds. Very small and unstable units made up of two to three platinum atoms are linked to the alumina surface and they show quite large intermetallic distances, the length being fixed by the carrier network at around 2.80 Å. When the formation of the cluster overcomes the bonding with oxygen, these distances come back to their normal value (2.75 Å) or less (2.70 Å) on increasing the temperature. The shortening of the Pt–Pt distance observed under these conditions is due to a decrease in the strength and rate of the hydrogen chemisorption on the metal atoms. Amplitudes of the thermal vibrations within the clusters increase with temperature and the hydrogen atoms encounter difficulties in interacting strongly with the metallic aggregates. There is consequently no compensation for the well-known distance contraction linked to the decrease in the particle size, a contraction which is relaxed when hydrogen exchanges bonds with platinum.

It was logical to extend this type of

0021-9517/90 $3.00

EXAFS work to the bimetallic couples that we have already studied either at the dried or at the calcined stage and we report here the analysis of data collected at the early stages of the reduction. This is an investigation of the metal particle genesis in order to check whether it follows the same trend as that found for the monometallic case (some epitaxy with the alumina network) and whether the second metal has any influence on the relationship.

EXPERIMENTAL

Synchrotron radiation from the DCI storage ring running at 1.85 GeV with an average current of 250 mA was used. The EXAFS data were collected on two stations. One was a conventional step-by-step setup with a channel cut (Si 331) monochromator and two ion chambers as detectors. The other associates dispersive optics provided by a bent crystal with a cooled photodiode array used as a position-sensitive detector (*10*). This last setup allows collection of a limited spectrum at once in less than 10 ms when a metallic foil is probed. The low concentrations we consider in our catalysts increase this time to a typical 10 to 15 s per spectrum (*11, 12*) instead of 10 min for a conventional setup.

The catalysts are highly dispersed Pt–(Re or Rh) systems deposited on γ-alumina extrudates (BET surface area 240 $m^2\ g^{-1}$) using the so-called pore-volume impregnation method. The different preparation parameters and sample characteristics are listed in Table 1.

For all the samples, we used a furnace with boron nitride holders similar to that designed by Lytle *et al.* (*13*). This device allows an *in situ* treatment of the catalysts without any contact with the atmosphere. It is important to note that in all cases the hydrogen flow begins simultaneously with the increase of the temperature.

The EXAFS spectra are recorded above the L_{III} edge of platinum (11560 eV) and analyzed in a conventional manner (*14*). The equation fitting the EXAFS oscillations, assuming no multiple scattering, is given by

TABLE 1

Sample Characteristics and Procedures for the Materials Considered for the Different Reductions

Preparation step	Catalyst	
	Pt–Re	Pt–Rh
Precursors	H_2PtCl_6 and NH_4ReO_4	H_2PtCl_6 and $RhCl_3, 3H_2O$
Impregnation	Successively	Simultaneously
Concentration (wt%)	0.5 Pt/0.11 Re	1.5 Pt/0.5 Rh
Drying	24 h at 110°C	24 h at 110°C
Calcination	24 h at 530°C	24 h at 530°C

$$\chi(k) = \frac{1}{k}\sum \frac{N_j}{R_j^2} F_j(k) e^{-2\sigma_j^2 k^2} e^{-\Gamma k/R} \sin(2kR_j + \Psi_j(k)),$$

where k is the wave vector of the ejected photoelectron. The sum is over shells containing N_j atoms at a distance R_j from the absorbing atom. The amplitude and phase shift ($F_j(k)$, $\Psi_j(k)$) parameters associated with the basckscattering process are extracted from reference compounds. σ_j is the relative displacement of the atoms, namely the Debye–Waller factor, arising from both static and dynamic disorder. In fact, we measure the variation of σ compared to its value in the standard. Finally, we used a two-shell least-squares fitting procedure to extract the values of N, R and $\Delta\sigma$. The photoelectron mean free path, Γ, has been fixed to its value in the standard, its influence being quite negligible in our cases.

RESULTS

Two kinds of information were extracted from the data. Qualitative information is provided by the well-known change in the white line intensity with the occupation of the metal 5*d* band (*15*). This correlation is parameterized by measuring the height of the white line, H. The plot of this parameter H versus time gives some indication of the

kinetic change of the platinum electronic state (*16*). Quantitative results are given by the EXAFS analysis, and a common way to visualize the evolution of the metal environment during the reaction is first to plot the magnitude of the Fourier transform (FT) of the EXAFS oscillations. In our case, we used a k^3 weighted Fourier transform. This quantity can be related to a radial distribution function with one platinum atom at $R = 0$ Å. Even at this step of the analytical procedure, it is easy to follow the structural modifications around the platinum atom, as the moduli of the pure compounds which limit the transformation, i.e., H_2PtCl_6, PtO_2, and Pt are very different.

We start by considering the direct reduction of a dried $Pt–Rh/Al_2O_3$ catalyst. The experimental setup used in this case was the dispersive one and spectra were recorded every minute. We first increased the temperature up to 100°C, the sample being under flowing hydrogen. The rate of temperature increase was around 3°C/min so that this operation took around 30 min. The sample was then stabilized at 100°C in order to limit the kinetics of the reduction. Despite the narrowness of the usable energy bandwidth (200 eV), a fact which explains the absence of numerical results, this experiment shows clearly the different steps of the reduction process. These qualitative features have been completed a second time by a study with a conventional setup of two $Pt–Re/Al_2O_3$ catalysts, one dried and the other calcined before being reduced. The two samples were under flowing hydrogen and the temperature had been increased to 275°C (about 2°C per minute) and 300°C (around 1.3°C per minute) for the dried and calcined starting catalysts, respectively.

A. Direct Reduction of a Pt–Rh/Al₂O₃ Catalyst

In the initial phase, the average platinum environment measured from spectra taken with a conventional setup is made up of 5.1 chlorines at 2.32 Å and 2.2 oxygens at 2.04 Å. The environment of these isolated complexes does not change during the first 30 min of the hydrogen treatment when the temperature is increased to 100°C (spectra 1 to 30 in Fig. 1). This is shown by:

(i) the shape and position of the FT which remain the same;

(ii) the absence of substantial changes observed in the Pt–Pt contribution coming from the presence of neighboring $PtCl_6^{2-}$ units, as indicated by the arrow in Fig. 1. The FT of spectrum 15, however, denotes that this contribution may disappear from time to time, a sign of some mobility for these entities onto the alumina surface.

From spectra 30 to 37 (Fig. 2), the mixed chlorine–oxygen neighboring starts to decrease regularly, the chlorine depopulation being easier to see than that of the oxygen.

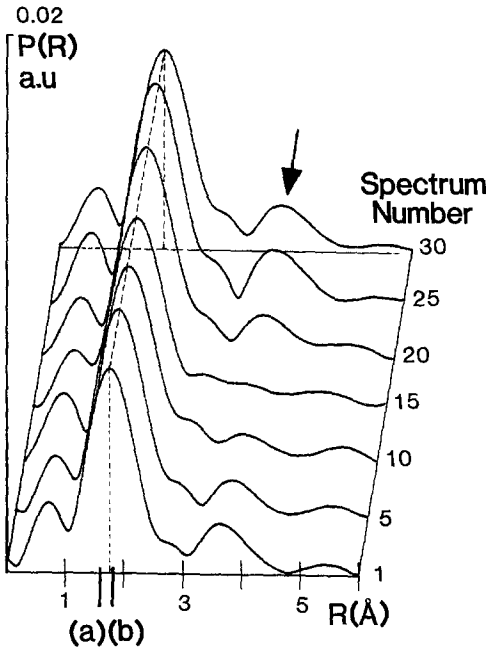

FIG. 1. Reduction of the dried $Pt–Rh/Al_2O_3$ catalyst: FT moduli changes at the Pt L_{III} edge during the first 30 min of treatment. The dotted line visualizes the mean distance of the initial Pt–(Cl,O) environment, (a) and (b) being the positions uncorrected for phase shift of the Pt–O and Pt–Cl pairs, respectively. The arrow indicates the place where the Pt–Pt contribution from the $PtCl_6^{2-}$ neighboring complexes emerges.

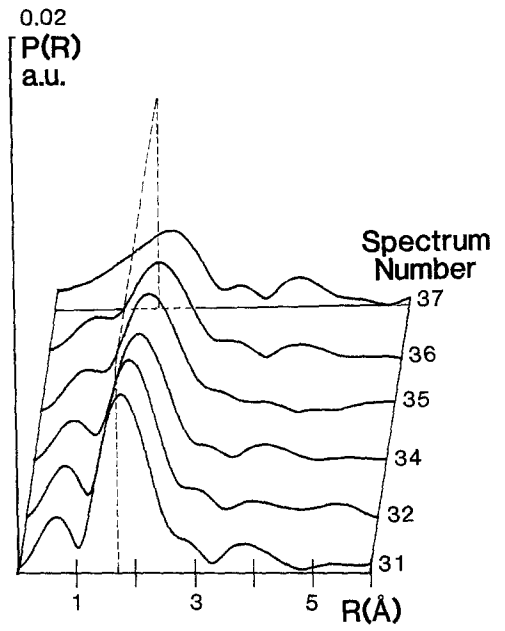

FIG. 2. As Fig. 1, but during the 7 min which follow. The mixed chlorine–oxygen environment of platinum begins to change regularly, the successive FT maxima moving away from the Pt–(Cl,O) starting position and intensity (dotted line).

All these points are in favor of a homogeneous decomposition of the $PtCl_6^{2-}$ unit. The temperature where the reduction process occurs is far less than the temperature observed in the monometallic case (210°C), a result of the rhodium effect on the platinum to alumina relationship. This agrees with temperature-programmed reduction measurements made by Ferretti (*17*), who showed that, after a 300°C calcination, pure rhodium catalysts start to reduce at low temperature, the maximum of the curve of hydrogen consumption peaking at 90°C and the reaction ending at 200°C. In the bimetallic system, rhodium is thus expected to reduce first and then to catalyze the reduction of the $PtCl_6^{2-}$ complexes. This difference in temperature with the pure platinum catalyst depends also on the total chlorine content of the catalysts, a point we have recently studied in detail (*6*).

The shape and position of spectra 38 to 42 indicate directly that when the number of neighbors is small (less than four), the situation becomes more complicated (Fig. 3). If the amplitude continues to diminish, the Pt–(Cl,O) distance can vary irregularly (compare here spectrum 40 with spectrum 39 or 41 which are taken 1 min before or after, respectively). This is in fact an illustration of the local chemical inhomogeneity present at this stage of the reduction, various species existing simultaneously with different stabilities, and equilibrium depending on the local partial pressure of various components such as hydrogen, chlorine, or HCl and water. An alternative explanation of these sudden changes might be the fact that we are not measuring the same part of the sample, as the size of the incoming beam is at least a factor of 10 less than for a conventional step-by-step experiment. We are not in favor of the latter explanation for two main reasons: first, it would mean that the sample will noticeably move within the cell, under the hydrogen

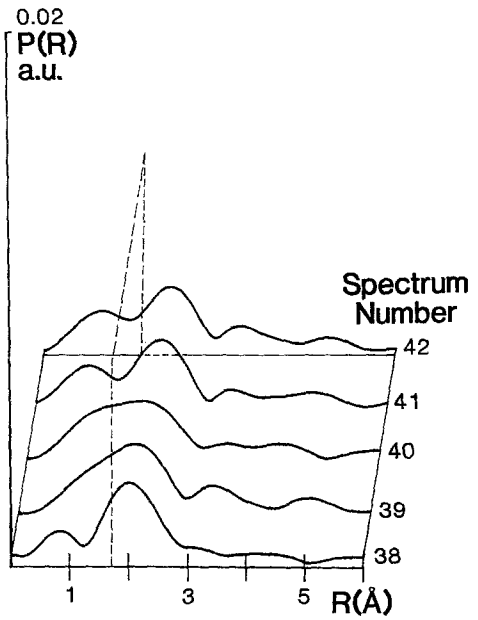

FIG. 3. As Fig. 2, but continuing for 5 min: irregular variations of the Pt–(Cl,O) first shell into Pt–Pt bonds can be seen.

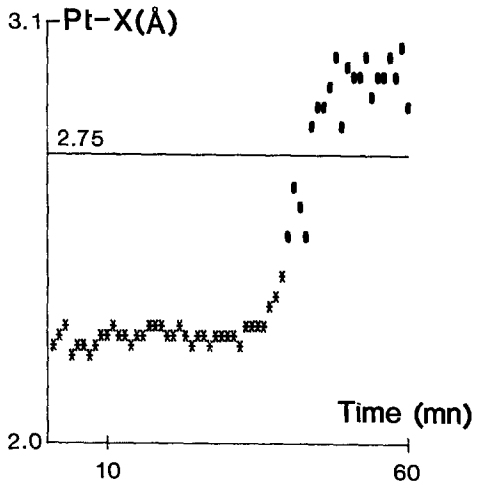

FIG. 4. Reduction of the dried $Pt–Rh/Al_2O_3$ catalyst: shift of the platinum to first-neighbor distances versus time. The horizontal line is the metallic Pt–Pt bond length (2.75 Å).

flow. The care we take to fill the container and then to purge the sample with the gas eliminates this occurrence, the compactness of the powder remaining strong enough to minimize the displacement of the grains. If the grains do suffer any movement, they are still largely located within the diameter of the X-ray beam. The second reason is related to the beam size itself: the operating conditions we choose to run the experiments (curvature of the crystal, adjustment of the sample at the focusing point) lead to a beam diameter of 1 to 2 mm, a dimension large enough to minimize any eventual displacement of the grains. In fact, upon opening the container at the end of each experiment, we saw no evidence for any holes in the catalyst bed. Spectra 39 and especially number 40, show the occurrence of a nonnegligible amount of oxygen in the vicinity of platinum. It looks as if PtO_x phases are needed as ignition compounds for the reduction, all these instabilities being related to the hydrogen flux. A qualitative analysis based on the position of the maxima of the FT moduli gives the point where the first platinum–platinum pairs are formed: Fig. 4 illustrates this where the circles replace the stars. An interesting feature is the Pt–Pt shift toward distances higher than the normal value of 2.75 Å measured in the bulk.

B. Reduction of a Dried $Pt–Re/Al_2O_3$ Catalyst

In this case we used a conventional setup, and a double analysis has been made (i) by measuring the evolution of the white line intensity and (ii) by fitting the EXAFS signals. This offers the opportunity to see whether any kinetic correlations exist between the electronic change in the platinum atoms and the structural modifications of their nearest environment.

Figure 5 shows the evolution of the white line intensity H as a function of time. The platinum atoms keep their initial electronic state until there is a clear change, seen over a few minutes, leading to the metallic state. Table 2 lists the corresponding numerical analysis of the EXAFS signals. One can see that at the beginning of the reaction, a constant chlorine–oxygen environment is observed from spectra 1 to 10. Basically, an average of three chlorine atoms at 2.32 Å and four oxygens at 2.00 Å define the first coordination sphere of platinum atoms. The variations in the structural parameters are

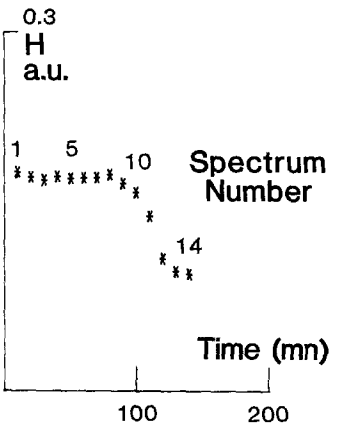

FIG. 5. Reduction of the dried $Pt–Re/Al_2O_3$ catalyst: change in the white line intensity H as a function of time.

TABLE 2

Changes in Platinum Neighbors during the Reduction of a Dried Pt–Re Catalyst

Spectrum number	Reduction time (min)	T (°C)	Chlorine			Oxygen			Platinum		
			N	R (Å)	$\Delta\sigma$ (Å)	N	R (Å)	$\Delta\sigma$ (Å)	N	R (Å)	$\Delta\sigma$ (Å)
1	10	24	3.3	2.32	0.02	4.4	2.00	0.01	None detectable		
2	20	30	3.2	2.34	0.02	4.3	2.04	0.00	None detectable		
3	30	34	3.4	2.31	0.00	3.6	2.04	0.02	None detectable		
4	40	46	3.4	2.31	0.02	4.0	2.00	0.00	None detectable		
5	50	84	2.8	2.31	0.02	4.1	2.03	0.01	None detectable		
6	60	109	2.9	2.35	0.02	4.2	2.05	0.01	None detectable		
7	70	130	3.3	2.32	0.02	4.4	2.03	0.00	None detectable		
8	80	148	2.8	2.32	0.02	4.0	2.04	0.00	None detectable		
9	90	174	3.5	2.34	0.00	3.6	2.03	0.00	None detectable		
10	100	242	3.3	2.37	0.02	3.7	2.06	0.02	None detectable		
11	110	264	1.9	2.34	0.02	3.7	2.06	0.01	None detectable		
12	120	271	2.0	2.30	0.02	None detectable			1.5	2.85	0.01
13	130	275	1.3	2.31	0.02	None detectable			3.4	2.80	0.03
14	140	277	1.0	2.32	0.02	None detectable			4.4	2.74	0.03

within the experimental errors, which are 0.03 Å for the interatomic distance R, 0.7 for the number of atoms N, and 0.02 for the Debye–Waller factor $\Delta\sigma$. Then, the total coordination decreases to the very low value of 2.6 instead of 6 to 7. This loss of ligands precedes the appearance of the first platinum to second metal bonds. We have here to make three important statements related to the creation of these platinum–metal pairs:

(i) The number of both Pt–Cl and Pt–O bonds decreases around this point, but the chlorine linkages are less affected: N_{Pt-Cl} changes from around 3 (spectra 8, 9, 10, Table 2) to 1 (spectra 13, 14), whereas no Pt–O bonds are detectable in spectra 12, 13, 14, although we measured almost four of them in spectra 8, 9, 10, and 11. The creation of platinum–metal pairs seems to be preferentially related to platinum–oxygen bond breaking, a point which has been previously noted for the pure platinum case. It was also qualitatively observed in the preceding reduction of the Pt–Rh/Al_2O_3 catalyst.

(ii) The contraction of the interatomic metal distance already seen after the reaction took place is not measured. On the contrary, we find again here an enlargement of the platinum to the second metal interatomic distance: spectrum 12 is, for example, well fitted by the contribution of two chlorines at 2.30 Å and 1.5 platinum at 2.85 Å. Figure 6 is an illustration of this phenomenon. It plots the different moduli (k^3 weighted and uncorrected for phase shifts) of experimental spectrum 14 (curve (1)) with the theoretical contributions of 4.5 platinum (curve (2)), one chlorine (curve (3)), and one oxygen atom (curve (4)). At this stage of the analysis it is already clear that oxygen backscattering does not contribute to the signal coming from the reduced catalyst (curve (1)). Part (I) of Fig. 7 thus represents the adjustment of curve (1) in the R-space (for both the magnitude as well as the imaginary part, the experimental data being given as the full line), Part (II) being the same fit but shown in the k space. They both give illustrations of the accuracy we look for in our analytical procedure; the numerical results are listed in Table 2.

(iii) The kinetics of the electronic change are faster than the structural reconstruction. This means that the platinum species

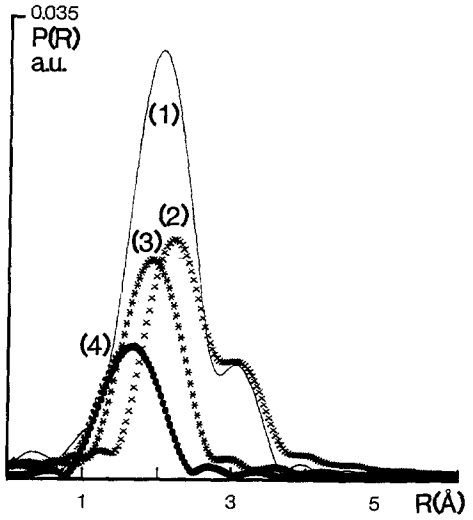

FIG. 6. Reduction of the dried Pt–Re catalyst: different moduli of Pt–neighbor pairs are shown: curve (1) is the experimental signal collected at 277°C after 140 min of reduction. Curves (2), (3), and (4) are contributions from 4.5 platinum, 1 chlorine, and 1 oxygen, respectively: it is clear that oxygen is not contributing to the experimental signal.

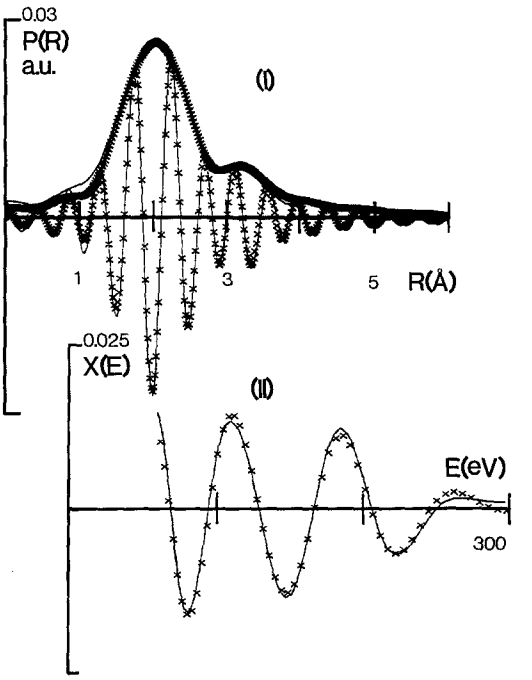

FIG. 7. Reduction of the dried Pt–Re catalyst: typical example of the agreement between an experimental run (full line) and its simulation (crossed line). (I) is curve (1) of Fig. 6 (modulus and imaginary part of the Fourier transform uncorrected for phase shift). (II) is the same adjustment shown in the energy space.

take on a certain metallic character within a structure which is not yet the well developed network of the metal.

C. Reduction of a Calcined Pt–Re/Al_2O_3 Catalyst

The conventional setup has again been used; the EXAFS results are gathered in Table 3 and Fig. 8 displays some of the corresponding FT moduli. Contrary to the former case, the initial environment of platinum changes as soon as the reduction starts, while the oxygen number decreases slowly, the chlorine number remaining constant. To explain this difficult removal of the chlorine from the platinum environment, we must remember that these platinum–chlorine bonds have resisted the calcination process. The result is that, contrary to the dried samples, several kinds of species exist after this step on the surface of the carrier. There are probably isolated complexes, as well as large PtO_2 particles. All this will lead to a spread in

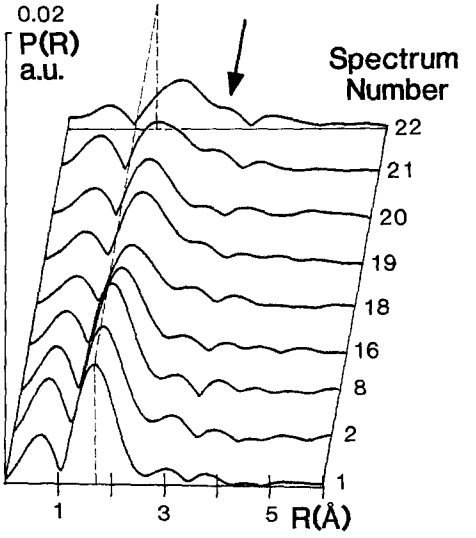

FIG. 8. Reduction of the calcined Pt–Re/Al_2O_3 catalyst: some of the experimental spectra are displayed to visualize the evolution of the starting complex (dashed line) into a small platinum cluster. The arrow points out the position of the long Pt–Pt bond length.

TABLE 3

Changes in Platinum Neighbors during the Reduction of a Calcined Pt–Re Catalyst

Spectrum number	Reduction time (min)	T (°C)	Chlorine			Oxygen			Platinum		
			N	R (Å)	$\Delta\sigma$ (Å)	N	R (Å)	$\Delta\sigma$ (Å)	N	R (Å)	$\Delta\sigma$ (Å)
1	10	16	1.5	2.33	0.02	4.1	2.00	0.00	None detectable		
2	20	16	1.5	2.34	0.02	3.8	2.01	0.00	None detectable		
3	30	16	1.5	2.33	0.00	4.0	2.01	0.02	None detectable		
4	40	25	1.5	2.33	0.02	3.8	2.01	0.00	None detectable		
5	50	36	1.4	2.33	0.02	3.9	2.01	0.02	None detectable		
6	60	51	1.5	2.32	0.02	3.8	2.01	0.00	None detectable		
7	70	70	1.5	2.35	0.02	4.3	2.00	0.00	None detectable		
8	80	89	1.5	2.35	0.02	3.8	2.02	0.01	None detectable		
9	90	108	1.5	2.33	0.00	3.4	2.00	0.02	None detectable		
10	100	139	1.8	2.35	0.00	2.9	2.00	0.00	None detectable		
11	110	147	1.5	2.35	0.00	3.3	2.00	0.02	None detectable		
12	120	156	1.5	2.31	0.02	2.7	2.00	0.02	None detectable		
13	130	168	1.7	2.33	0.02	3.0	1.99	0.02	None detectable		
14	140	183	1.5	2.34	0.02	3.2	1.99	0.02	None detectable		
15	150	198	1.6	2.35	0.00	2.7	2.00	0.00	None detectable		
16	160	213	1.1	2.35	0.02	2.7	2.03	0.01	None detectable		
17	170	231	1.4	2.38	0.03	2.1	1.99	0.02	None detectable		
18	180	244	1.4	2.38	0.01	2.1	1.99	0.02	None detectable		
19	190	252	1.4	2.36	0.00	1.5	2.03	0.00	None detectable		
20	200	262	1.2	2.36	0.00	1.5	2.00	0.00	None detectable		
21	210	275	1.5	2.26	0.02	None detectable			3.4	2.81	0.03
22	220	305	1.5	2.28	0.02	None detectable			4.8	2.79	0.05

reducibility and thus to a continuous, rather than to an abrupt, decrease in the number of oxygen neighbors. This continuous decrease in the number of oxygens seems in line with the fact that the reduction of a calcined sample is made up of a succession of small structural modifications. This is illustrated in Fig. 9 which is the plot of the change in the white line intensity H versus time: the change here is monotonic and does not show the sudden variation we measured during the reduction of the dried sample (Fig. 5). Although the reduction of the oxidized species is softer than that of the chlorinated species, it leads nevertheless to the same phenomenon: the loss of ligands is once more accompanied by the formation of long platinum-to-second-metal bonds. This is visualized in Fig. 8 by the existence of a shoulder on the right side of the first coordination peak (arrowed on spectrum 22). The intensity of this feature is quite important compared to that of the main peak and the different conditions we

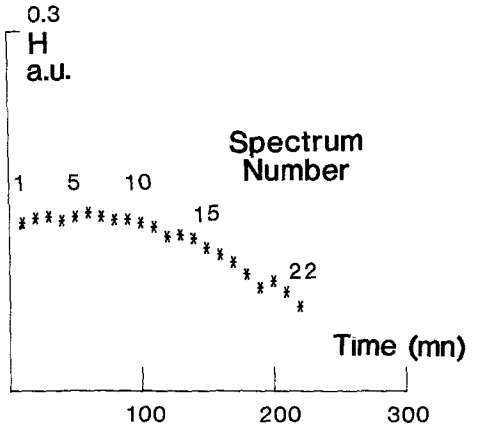

FIG. 9. Reduction of the calcined Pt–Re/Al_2O_3 catalyst: change in the white line intensity H as a function of time.

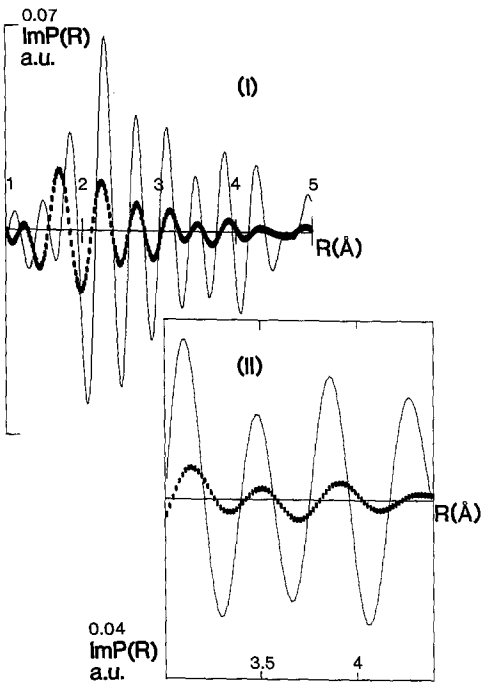

FIG. 10. Imaginary part of the FT of spectrum 21 (calcined Pt–Re catalyst). (II) is an enlargement between 3 and 4.4 Å of (I), which illustrates the shift toward long Pt–Pt distances.

used to Fourier transform the experimental signals definitely ensure that such a lobe is not produced by any spurious mathematical treatment. Fitting the corresponding filtered $k^3\ \chi(k)$ signal leads to an average of 1.5 chlorines at 2.27 Å and 4.1 metallic atoms at 2.80 Å for the first neighborhood of platinum.

Figure 10 provides evidence for the simultaneous presence of light and heavy elements around platinum. Part (I) is the imaginary part of the FT of spectrum 21 (black dots) and pure metallic foil (full line), the plot being given uncorrected for phase shift. The displacement toward a short distance presented between 1 and 2.5 Å is very clear and chlorine has been determined to be the main atom which contributes to this effect, as the result of the adjustment is better than when oxygen is considered. The Pt–Cl distance of 2.26 Å which we found is however slightly shorter than the normal value of 2.32 Å, a point which could indicate that a few oxygens are still remaining in this signal. Part (II) is a magnification of part (I) between 3 and 4.4 Å and shows unambiguously the existence of the long metal–metal distance. The effect is apparent not only on the first shell which is spreading up to around 3.5 Å under our analytical conditions (5.6 $Å^{-1}$ in the k space), but also on the higher shells as the shift in distance is still visible after this limit. The signal there is nevertheless too weak to be accurately analyzed.

On the other hand, the energy bandwidth used in our analysis, no matter what kind of reduction we made, from the dried or the calcined samples, is another limitation of the accuracy of the results. These drawbacks, however, are counterbalanced by the fact that the nature of the first backscatterers which surround platinum is very different: (i) low Z elements such as chlorine and/or oxygen and (ii) high Z elements such as platinum and/or rhenium. There is no difficulty in clearly separating their respective contribution to the experimental signal: at this step of the analysis we systematically considered the plots of $\log[\chi(\text{catalyst})/\chi(\text{platinum foil})]$ as a function of k^2, a test which is very sensitive in proving the existence of a light element in the coordination sphere of platinum.

The main problem we encountered came from an eventual differentiation between oxygen and chlorine atoms (the Pt and Re backscattering atom contributions in any case cannot be separated) during the reduction of calcined samples. Even though there is a total phase shift between the two Pt–O and Pt–Cl pairs around 200 eV after the absorption edge, we consider that the number of neighboring atoms is too small to make significant three subshell (Pt–O, Pt–Cl, and Pt–Pt) fitting operations. Spectra 21 and 22 (Table 3) show the results of several tests we made to decide which was the main light atom contributor, using only two subshells in the fitting procedure by comparing the

results of a (Pt–O) + (Pt–Pt) combination with those of a (Pt–Cl) + (Pt–Pt) combination. It appears that the reliability factor was largely reduced in the second case (Pt–Cl neighbors). If some Pt–O contributions were subsequently introduced into the calculation, the agreement with the experimental signal became worse. We therefore associated the disappearance of Pt–O bonds with the simultaneous formation of the first Pt–Pt pair. However, as we already pointed out, the Pt–Cl bond length is shortened compared with the reference value, a point which could be interpreted as fewer oxygen atoms remaining in the vicinity of platinum.

DISCUSSION

The primary new result of these investigations is to give evidence for a relationship between the metal cluster and the carrier through the measurement of an abnormally long metal–metal interatomic distance. This is contrary to the well-known contraction of the nearest neighbor distance which occurs in small metal aggregates. Apai *et al.* (*18*) have for example shown bond shortening from the EXAFS measurements they made on small Cu and Ni clusters. This collapse is also in line with theoretical studies (*19, 20*) which use an approximation based on the second moment of the density of states to calculate the cohesive energy (*21*).

A few years ago, Balerna *et al.* (*22*) pointed out that this contraction was accompanied by an increase in the Debye–Waller factor. The disorder we consider in our fitting procedure assumes that the motion of neighboring atoms is small and harmonic. Such an assumption, however, is not really valid for nanometric clusters. As a matter of fact Lytle *et al.* (*23*) demonstrated that, in the case of platinum deposited on SiO_2, the disorder, when extrapolated to the temperature of 0 K, remains considerably larger than that for bulk platinum. Similar experiments led Marques *et al.* (*24*) to the conclusion that the disorder measured for the catalyst is 1.3 to 2 times more than the value determined for bulk platinum over all temperatures.

The effect of high disorder on the EXAFS formula has in fact been extensively studied (*25–27*). When one accounts for anharmonic contributions, an accurate determination of interatomic distances and mean square relative displacements can be made. The conclusion which must be underlined is that the inadequate representation of thermal disorder in the EXAFS equation leads to an underestimation of the nearest neighbor distance. As our analytical procedure takes into account solely a small quantity of disorder, the former remarks reinforce the existence of the long metal–metal bond length we found for the small nucleus made up of three to four heavy atoms.

Particular attention must be paid also to the presence of hydrogen. Its chemisorption may influence the amplitude of the contraction. Moraweck and Renouprez (*28*) have determined for small platinum particles encaged in the framework of a Y-zeolite, a contraction of 3% of the nearest neighbor distance when the catalyst was placed under vacuum. This contraction disappears upon hydrogen chemisorption. If the sample is observed at high temperature, a contraction still exists as shown by one of us (*8*) in the case of platinum supported on alumina. The long metal–metal distance cannot therefore be explained by hydrogen chemisorption.

The only assumption which remains to explain this abnormal interatomic metal distance is that the platinum clusters can be considered in epitaxy with the support. This conclusion is based on the hypothesis that the platinum atoms occupy adjacent threefold hollow sites above the (111) oxygen surface layer of the carrier where the atoms are separated by 2.8 Å. Such an intergrowth has already been observed for palladium on γ-alumina (*29*) by microdiffraction experiments using a scanning transmission electron microscope. The par-

ticle and a large area of the carrier which surrounds it are in the same orientation when the impregnation procedure is not too destructive of the surface of the alumina.

CONCLUSION

Different catalysts, mono- or bimetallic, previously dried or calcined, have been investigated during the genesis of the first metal clusters which appear at the beginning of the reduction process. The observations were made *in situ*, as a function of time, on the scale of a few seconds or a few minutes. All the measurements lead to the same result: when the very first metallic atoms gather to form the nucleus of the cluster, the strength of the bonds they exchange through chlorine or oxygen with their support is great enough to impose a continuity with the network of the carrier. This effect is revealed by an enlargement of the metal–metal distance whose value becomes close to the (111) interplanar distance of alumina. This phenomenon seems therefore to be general, whatever the second metal associated with platinum. When the reduction time increases, this intergrowth becomes weaker and the construction of a normal metallic cluster may start. If a bimetallic couple is considered, the metal segregation often encountered then comes later on, the duration of all these successive steps depending on many parameters such as the hydrogen pressure, the total chlorine content, and the temperature at which the reduction has been performed.

ACKNOWLEDGMENTS

Thanks are due to the team in charge of the DCI storage ring who ran the equipment during the experiments. We are also very grateful to our colleagues who developed the dispersive mode station, in particular M. E. Dartyge who made the original setup we used in the present series of experiments.

REFERENCES

1. Lytle, F. W., Sayers, D. E., and Moore, E. B., *J. Appl. Phys. Lett.* **24,** 45 (1974).
2. Lagarde, P., and Dexpert, H., *Adv. Phys.* **33,** 567 (1984).
3. Bart, J. C. J., and Vlaic, G., *Adv. Catal.* **34** (1985).
4. Koningsberger, D. E., and Prins, R., *in* "X-Ray Absorption: Principles, Applications, Techniques of EXAFS, SEXAFS and XANES," Chemical Analysis Ser. Wiley, New York, 1987.
5. Bazin, D., Dexpert, H., Lagarde, P., and Bournonville, J. P., *J. Catal.* **110,** 209 (1988).
6. Bazin, D., Dexpert, H., Guyot-Siommest, N., Bournonville, J. P., and Lynch, J., *J. Chem. Phys.* **86,** 1707 (1989).
7. Bazin, D., Dexpert, H., Lagarde, P., and Bournonville, J. P., *J. Phys.* **47,** 293 (1986).
8. Dexpert, H., *J. Phys.* **47,** 219 (1986).
9. Lenormand, F., Bazin, D., Dexpert, H., Lagarde, P., and Bournonville, J. P., *in* "Proceedings, 9th International Congress on Catalysis, Calgary, 1988" (M. J. Phillips and M. Ternan, Eds.). Chem. Institute of Canada, Ottawa, 1988.
10. Dartyge, E., Depautex, C., Dubuisson, J. M., Fontaine, A., Jucha, A., Leboucher, P., and Tourillon, G., *Nucl. Instrum. Methods Phys. Res.* **246,** 452 (1986).
11. Sayers, D. E., Bazin, D., Dexpert, H., Jucha, A., Dartyge, E., Fontaine, A., and Lagarde, P., *in* "EXAFS and Near Edge Structure III" (K. Hodgson, B. Hedman, and J. Penner-Hahn, Eds.), p. 209. Springer-Verlag, Berlin, 1984.
12. Maire, G., Garin, F., Bernhardt, P., Girard, P., Schmitt, J. L., Dartyge, E., Dexpert, H., Fontaine, A., Jucha, A., and Lagarde, P., *Appl. Catal.* **26,** 305 (1986).
13. Lytle, F. W., Weip, S. P., Greegor, R. B., Via, G. H., and Sinfelt, J. H., *J. Chem. Phys.* **70,** 4849 (1979).
14. Lagarde, P., Murata, F., Vlaic, G., Freund, E., Dexpert, H., and Bournonville, J. P., *J. Catal.* **84,** 333 (1983).
15. Mansour, A. N., Cook, J. W., Jr., Sayers, D. E., *J. Phys. Chem.* **88,** 2330 (1984).
16. Bazin, D., Dexpert, H., and Lagarde, P., Topics in Current Chemistry, No. 145, p. 70. Springer-Verlag, Berlin, 1988.
17. Ferretti, O. A., PhD thesis, University of Paris VI, 1976.
18. Apai, G., Hamilton, J. F., Stohr, J., and Thomson, A., *Phys. Rev. Lett.* **43,** 165 (1979).
19. Gordon, M. B., Cyrot-Lackmann, F., and Desjonqueres, M. C., *Surf. Sci.* **80,** 159 (1979).
20. Khanna, S. N., Bucher, J. P., Buttet, J., and Cyrot-Lackmann, F., *Surf. Sci.* **127,** 165 (1983).
21. Ducastelle, F., *J. Phys.* **31,** 1055 (1970).
22. Balerna, A., Bernieri, E., Piccozzi, P., Beale, A., Santucci, S., Burattini, E., and Mobilio, S., *Surf. Sci.* **156,** 206 (1985).
23. Lytle, F. W., Greegor, R. B., Marques, E. C., Sandstrom, D. R., Via, G. H., and Sinfelt, J. H., *J. Catal.* **95,** 546 (1985).
24. Marques, E. C., Sandstrom, D. R., Lytle, F. W.,

and Greegor, R. B., *J. Chem. Phys.* **77,** 1027 (1982).

25. Eisenberger, P., and Brown, G. S., *Solid State Comm.* **28,** 481 (1979).
26. Tranquada, J. M., *in* "EXAFS and Near Edge Structure III" (K. Hodgson, B. Hedman, and J. Penner-Hahn, Eds.), p. 74. Springer-Verlag, Berlin, 1984.
27. Greegor, R. B., and Lytle, F. W., *Phys. Rev. B* **20,** 4902 (1979).
28. Moraweck, B., and Renouprez, A. J., *Surf. Sci.* **106,** 35 (1981).
29. Dexpert, H., Freund, E., Lesage, E., and Lynch, J. P., *in* "Metal-Support and Metal-Additive Effects in Catalysis" (B. Imelik *et al.,* Eds.), p. 53. Elsevier, Amsterdam, 1982.